4096 *Chem. Mater.* **2010,** *22,* 4096–4102
DOI:10.1021/cm100998e

CHEMISTRY OF MATERIALS
Article

Polypropylene/Graphene Oxide Nanocomposites Prepared by In Situ Ziegler−Natta Polymerization

Yingjuan Huang,[†,‡] Yawei Qin,[†,‡] Yong Zhou,[†] Hui Niu,[†] Zhong-Zhen Yu,*[,§] and Jin-Yong Dong*[,†]

[†]*CAS Key Laboratory of Engineering Plastics, Joint Laboratory of Polymer Science and Materials, Institute of Chemistry, Chinese Academy of Sciences, Beijing 100190, China,* [‡]*Graduate School, Chinese Academy of Sciences, Beijing 100049, China, and* [§]*Beijing Key Laboratory on Preparation and Processing of Novel Polymeric Materials, Department of Polymer Engineering, College of Materials Science and Engineering, Beijing University of Chemical Technology, Beijing 100029, China*

Received April 10, 2010. Revised Manuscript Received June 3, 2010

This paper reports the first example of preparation of polypropylene/graphene oxide (PP/GO) nanocomposites via in situ Ziegler−Natta polymerization. A Mg/Ti catalyst species was incorporated into GO via surface functional groups including −OH and −COOH, giving a supported catalyst system primarily structured by nanoscale, predominantly single GO sheet. Subsequent propylene polymerization led to the in situ formation of PP matrix, which was accompanied by the nanoscale exfoliation of GO, as well as its gradual dispersion. Morphological examination of the ultimate PP/GO nanocomposites by TEM and SEM techniques revealed effective dispersion in nanoscale of GO in PP matrix. High electrical conductivity was discovered with thus prepared PP/GO nanocomposites; for example, at a GO loading of 4.9 wt %, σ_c was measured at 0.3 $S \cdot m^{-1}$.

Introduction

Graphene oxide (GO), basically graphene bearing generally hydroxyl and carboxyl functional groups, is a layered carbon nanomaterial produced by the oxidation of natural graphite flakes, followed by ultrasonication treatment of its aqueous solution.[1] Since GO is chemically similar to carbon nanotube and structurally analogous to layered clay,[2] it has a great potential to simultaneously improve not only the mechanical and barrier properties but also functional properties like electrical and thermal conductivities of polymers.[3] Despite the potential advantages, the synthesis of GO-reinforced polymer nanocomposites was challenging in obtaining well-dispersed GO sheets in polymer matrix, especially when the polymer is selected from nonpolar polymer category typically represented by a polyolefin like PE or PP. Generally, solution mixing is one ideal way to polymer/GO nanocomposites provided the polymer is readily soluble in common organic solvents. Such polar polymers as PMMA, PAN, PAA, and polyesters have been successfully applied in nanocomposite fabrication with GO using this art.[4,5] This approach was recently further boosted via GO surface modification with reagents like alkylchlorosilanes, alkylamine, isocyanates, etc.[6−8] For instance, GO was isocyanate-treated in DMF and mixed with polystyrene to form polystyrene/GO nanocomposites.[3a] Poly(vinyl alcohol) was mixed in DMSO with esterificated GO to fabricate PVA-based GO nanocomposites.[3g] Most recently, the solution method was also applied to prepare thermoplastic polyurethane (TPU)/GO nanocomposites.[3h] At the same time, melt

*To whom correspondence should be addressed. Tel:/Fax: 0086-10-82611905 (J.-Y.D.); 0086-10-64428582 (Z.-Z.Y.). E-mail: jydong@iccas.ac.cn (J.-Y.D.); yuzz@mail.buct.edu.cn (Z.-Z.Y.).

(1) (a) Hummers, W.; Offeman, R. *J. Am. Chem. Soc.* **1958**, *80*(6), 1339. (b) Boehm, H. P.; Scholz, W *Carbon* **1968**, *6*(2), 226–227. (c) Nakajima, T.; Mabuchi, A.; Hagiwara, R. *Carbon* **1988**, *26*(3), 357–361. (d) Lerf, A.; He, H.; Forster, M.; Klinowski, J. *J. Phys. Chem. B* **1998**, *102*(23), 4477–4482. (e) Shen, J.; Hu, Y.; Shi, M.; Lu, X.; Qin, C.; Li, C.; Ye, M. *Chem. Mater.* **2009**, *21*, 3514–3520.

(2) (a) Geim, A. K.; Novoselov, K. S. *Nat. Mater.* **2007**, *6*, 183–191. (b) Katsnelson, M. I. *Mater. Today* **2007**, *10*, 1–8. (c) de Heer, W. A.; Bergera, C.; Wu, X.; First, P. N.; Conrad, E. H.; Li, X.; Li, T.; Sprinkle, M.; Hass, J.; Sadowski, M. L.; Potemski, M.; Martinez, G. *Solid State Commun.* **2007**, *143*, 92–100. (d) Thostenson, E. T.; Li, C.; Chou, T. W. *Compos. Sci. Technol.* **2005**, *65*, 491–516.

(3) (a) Stankovich, S.; Dikin, D. A.; Dommett, G. H. B.; Kohlhaas, K. M.; Zimney, E. J.; Stach, E. A.; Piner, R. D.; Ngugen, S. T.; Ruoff, R. S. *Nature* **2006**, *442*, 282–286. (b) Causin, V.; Marega, C.; Marigo, A.; Ferrara, G.; Ferraro, A. *Eur. Polym. J.* **2006**, *42*, 3153–3161. (c) Kalaitzidou, K.; Fukushima, H.; Drzal, L. T. *Composites, Part A* **2007**, *38*, 1675–1682. (d) Kalaitzidou, K.; Fukushima, H.; Drzal, L. T. *Carbon* **2007**, *45*, 1446–1452. (e) Szabo, T.; Szeri, A.; Dekany, I. *Carbon* **2005**, *43*, 87–94. (f) Xu, J.; Hu, Y.; Song, L.; Wang, Q.; Fan, W.; Chen, Z. *Carbon* **2002**, *40*, 445–467. (g) Salavagione, H. J.; Gomez, M. A.; Martnez, G. *Macromolecules* **2009**, *42*, 6331–6334. (h) Nguyen, D. A.; Lee, Y. R.; Raghu, A. V.; Jeong, H. M.; Shinb, C. M.; Kim, B. K. *Polym. Int.* **2009**, *58*, 412–417.

(4) Ramanathan, T.; Abdala, A. A.; Stankovich, S.; Dikin, D. A.; Herrera-alonso, M.; Piner, R. D.; Adamson, D. H.; Schniepp, H. C.; Chen, X.; Ruoff, R. S.; Nguyen, S. T.; Aksay, I. A.; Prudhomme, R. K.; Brinson, L. C. *Nat. Nanotechnol.* **2008**, *3*, 327–331.

(5) (a) Kim, H.; Macosko, C. W. *Macromolecules* **2008**, *41*, 3317–3327. (b) Debelak, B.; Lafdi, K. *Carbon* **2007**, *45*, 1727–1734.

(6) (a) Matsuo, Y.; Tabata, T.; Fukunaga, T.; Fukutsuka, T.; Sugie, Y. *Carbon* **2005**, *43*, 2875–2882. (b) Matsuo, Y.; Fukunaga, T.; Fukutsuka, T.; Sugie, Y. *Carbon* **2004**, *42*, 2113–2130.

(7) (a) Matsuo, Y.; Watanabe, K.; Fukutsuka, T.; Sugie, Y. *Carbon* **2003**, *41*, 1545–1550. (b) Matsuo, Y.; Miyabe, T.; Fukutsuka, T.; Sugie, Y. *Carbon* **2007**, *45*, 1005–1012. (c) Matsuo, Y.; Nishino, Y.; Fukutsuka, T.; Sugie, Y. *Carbon* **2007**, *45*, 1384–1390.

(8) (a) Stankovich, S.; Piner, R. D.; Nguyen, S. T.; Ruoff, R. S. *Carbon* **2006**, *44*, 3342–3347. (b) Xu, C.; Wu, X.; Zhu, J.; Wang, X. *Carbon* **2008**, *46*, 386–389.

 Published on Web 06/15/2010

mixing is also adoptable for polymer/GO nanocomposite fabrication, which in fact is applicable to not only those solvent-resolvable polar polymers but nonpolar polymers like polyolefins as well. For example, Macosko et al. employed a melt mixing method to successfully prepare poly(ethylene-2,6-naphthalate)/GO nanocomposites.[5a] As for nanocomposites based on polyolefins, several groups started from the prototype of GO - graphite - to prepare PP-based nanocomposite[3b−d] that, because of a poor exfoliation of graphite, resulted in only limited degree of property improvement. The graphite exhibited significant impacts on the mechanical properties of PP only at loadings higher than 5 vol %[3c] and on the thermal conductivity at contents over 20 wt.%.[3b] Only until recently has Torkelson and co-workers adopted a special method (solid-state shear pulverization, SSSP) to improve the exfoliation of graphite and produced PP/graphite nanocomposites with well-dispersed nano graphite sheets (graphene).[9]

Summarizing the existing reports on the preparation of PP/GO or graphene nanocomposites,[3b−d,9] it is perceivable that, because obtaining such nanocomposites is still so challenging a task, more suitable and convenient approaches deserve pursuit. As such, in this article, we exercise an in situ polymerization strategy to prepare PP/GO nanocomposites.

In the previous studies carried out by both ourselves and other groups, natural clays with surface modification have been successfully imbedded into chemically nonpolar polymers such as polyolefins by applying the in situ intercalative polymerization of olefins.[10] The approach is conducted by the intercalation of transition metal olefin polymerization catalysts (including Ziegler−Natta, metallocene, and postmetallocene) in the interlayer of an organically modified clay followed by an in situ olefin polymerization. It has the advantage of bypassing the thermodynamic or kinetic limitations associated with direct polymer intercalation, because olefin monomers of in situ polymerization can penetrate into the interlayer spaces of silicate more easily than polymers or macromolecules. Because of structural analogy to layered clay, the same methodology could be applied for synthesizing PP/GO or graphene nanocomposites. Because of the functional groups present in GO, the sorption and intercalation of molecules is possible,[11] which facilitates the intercalation of olefin polymerization catalysts into the intragallery of GO nanosheets.

Experimental Section

Materials. All O_2- and moisture-sensitive manipulations were carried out in argon atmosphere using standard Schlenk techniques. Hexane and tetrahydrofuran (THF) were deoxygenated by argon purge before being refluxed over sodium for 48 h and distilled before use. Triethyl aluminum (TEA, 1.8 mol/L in heptane) was purchased from Albermarle and used as received. Dimethoxydiphenylsilane (DDS, 0.089 mol/L in heptane) was purchased from Aldrich. Titanium tetrachloride ($TiCl_4$) and chloro-butane, both AR-grade, were purchased from Beijing Chemical Factory and were used without further purification. Polymerization-grade propylene was supplied by Yanshan Petrochemical Co. of China. Graphene oxide was prepared from natural graphite by the Hummers method.[1a]

Synthesis of GO-Supported Ziegler−Natta Catalyst. The Grignard reagent, C_4H_9MgCl (BuMgCl), was prepared by reaction between chlorobutane (10 mL) and magnesium powder (2.8 g) in tetrahydrofuran (50 mL) at refluxing temperature (80 °C) in N_2 atmosphere for 20 h. Then, 0.1 mol of BuMgCl/tetrahydrofuran solution was added dropwise into a 800 mL of tetrahydrofuran suspension containing 0.8 g GO. After 48 h of reaction at refluxing temperature (80 °C), the excess Grignard reagent was filtered off, and the solid was washed in turn with tetrahydrofuran and hexane for three times. The powdery product was dried under vacuum at 60 °C for 12 h, and 1.2 g BuMgCl/GO was obtained.

One gram of BuMgCl/GO was added into 50 mL $TiCl_4$ at room temperature, after which the temperature was brought up to 120 °C, and the mixture was stirred for 4 h. Then the reactant was filtered to remove the unreacted $TiCl_4$, and a second 30 mL volume of $TiCl_4$ was charged into the reactor. The reaction was completed after stirring for 4 h at 120 °C. The reaction mixture was filtered, washed with hot hexane six times, and dried under vacuum at 60 °C for 12 h; 0.9 g GO-supported Ziegler−Natta catalyst, $TiCl_4$/(BuMgCl/GO), was then rendered.

In Situ Propylene Polymerization. The polymerization reaction was carried out with a Parr stainless steel autoclave reactor equipped with a mechanical stirrer. In a typical reaction (entry PP2 in Table 1), 100 mL of hexane was added into the reactor, which was then filled with propylene under a constant pressure of 0.5 MPa. After the reactor had been heated to 60 °C, the powdery catalyst $TiCl_4$/(BuMgCl/GO) (0.038 g) was added into the vigorously stirred liquid mixture saturated with propylene. The polymerization reaction was initiated by charging $AlEt_3$ (0.6 mL, 1.08 mmol) and DDS (0.108 mmol) into the reactor using syringe. After 30 min, the polymerization was quenched by 20 mL of acidified ethanol (containing 10% HCl). The polymer product was collected by filtration, and repeatedly washed with ethanol and distilled water. After it was dried under vacuum at 60 °C for 24 h, 12.8 g of polymer product was obtained as a gray powder (PP/GO).

Characterization. Elemental analysis was performed on Flash EA 1112. Fourier transform-infrared spectroscopy (FTIR) was performed on a Perkin-Elmer system 2000 FTIR spectrometer, and the samples were prepared by cocompression of KBr powder with ~0.2 wt % GO or BuMgCl/GO. The particle morphology of samples was observed with a JEOL-S4300 and S4800 cold-field emission scanning electron microscopy (SEM). Ultrathin sections of the polypropylene nanocomposites were observed by Jeol JEM 2200FS and Jeol JEM 2011 transmission electron microscopes (TEM) at an accelerating voltage of 200 kV. The as-polymerized powder polymer samples were directly used for Raman spectroscopy measurement. X-ray photoelectron spectroscopy (XPS) data were obtained with an ESCALab220i-XL electron spectrometer from VG Scientific using 300W Al Ka radiation. The base pressure was about 3×10^{-9} mbar. The binding energies were referenced to the C1s line at 284.8 eV from

(9) Wakabayashi, K.; Pierre, C.; Dikin, D. A.; Ruoff, R. S.; Ramanathan, T.; Brinson, L. C.; Torkelson, J. M. *Macromolecules* **2008**, *41*, 1905–1908.
(10) (a) Huang, Y.; Yang, K.; Dong, J. Y. *Macromol. Rapid Commun.* **2006**, *27*, 1278–1283. (b) Huang, Y.; Yang, K.; Dong, J. Y. *Polymer* **2007**, *48*, 4005–4014. (c) Yang, K.; Huang, Y.; Dong, J. Y. *Polymer* **2007**, *48*, 6254–6261. (d) Sun, L.; Liu, J.; Kirumakki, S. R.; Schwerdtfeger, E. D.; Howell, R. J.; Al-Bahily, K.; Miller, S. A.; Clearfield, A.; Sue, H. -J. *Chem. Mater.* **2009**, *21*, 1154–1161.
(11) McAllister, M. J.; Li, J.-L.; Adamson, D. H.; Schniepp, H. C.; Abdala, A. A.; Liu, J.; Herrera-Alonso, M.; Milius, D. L.; Car, R.; Prud'homme, R. K.; Aksay, I. A. *Chem. Mater.* **2007**, *19*, 4396–4404.

Table 1. Conditions and Results of Propylene Polymerization Catalyzed by $TiCl_4$/(BuMgCl/GO)[a]

entry	TEA (mL)	*t* (min)	yield (g)	*A*[b]	GO content[c] (wt %)	M_η ($\times 10^5$ g/mol)	σ_c (S m^{-1})	T_m (°C)
PP1	0.2	30	1.14	0.35	0.96	7.5	4.80×10^{-8}	160.0
PP2	0.6	30	12.8	4.20	0.42	7.3	9.25×10^{-9}	160.3
PP3	0.6	8	4.12	4.83	1.52	7.7	9.33×10^{-4}	160.2
PP4	0.2	10	0.79	0.51	4.90	8.1	3.12×10^{-1}	160.9

[a] Other reaction conditions: 100 mL hexane, Al/Si = 10:1, 60 °C, 0.5 MPa. [b] *A* = activity $\times 10^7$ g PP/mol Ti·h. [c] Calculated based on the added GO amount.

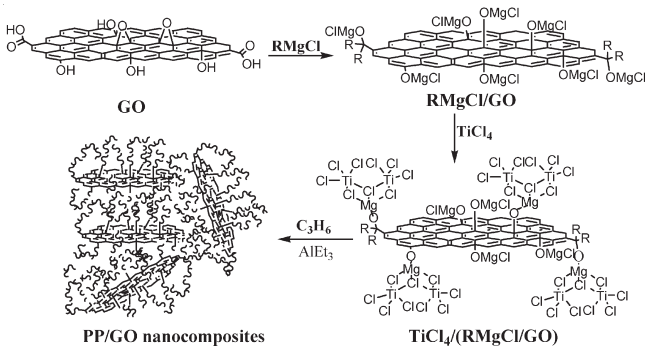

Figure 1. Fabrication of PP/GO nanocomposites by in situ Ziegler−Natta polymerization.

adventitious carbon. The crystallization and melting behaviors of polypropylene nanocomposites were characterized using a Perkin-Elmer DSC-7 differential scanning calorimeter under nitrogen atmosphere. All specimens were heated from 50 to 200 °C at a heating rate of 10 °C/min and kept for 10 min to erase the thermal history. The melt and crystallization behaviors were then recorded at heating or cooling rates of 10 °C/min. Melting temperature (T_m) was determined from the second heating scan. The intrinsic viscosity of polymers was measured in decalin at 135 °C with a Cannon-Ubbelohde viscometer. The viscosity-average molecular weight was calculated by the Marke-Houwink equation: $[\eta] = 1.1 \times 10^{-4} M_\eta^{0.8}$. Films with thicknesses around 0.3−0.5 mm were prepared by hot-compression of the polymerized products at 190 °C and their DC conductivities were measured by Keithley 4200 using a standard four probe method at room temperature. Equation 1 was used to calculate the electrical resistivity (ρ):

$$\rho = \frac{\Delta V w t}{i L} \quad (1)$$

where ΔV is the voltage drop over the center of the sample, w is the sample width, t is the sample thickness, i is the current, and L is the length over which ΔV is measured. Equation 2 was used to calculate the electrical conductivity (σ_c)

$$\sigma_c = \frac{1}{\rho} \quad (2)$$

Results and Discussion

In this paper, we fabricate PP/GO nanocomposites with well exfoliated and dispersed GO sheets by the in situ intercalative polymerization, based on a reaction scheme illustrated in Figure 1. First, a GO-supported catalyst, $TiCl_4$/(BuMgCl/GO), is synthesized through the reaction of a Grignard reagent BuMgCl with GO in THF, followed by an excessive $TiCl_4$ treatment to generate Mg/Ti catalyst species on GO individual sheet surface. Then the supported catalyst is engaged in propylene polymerization

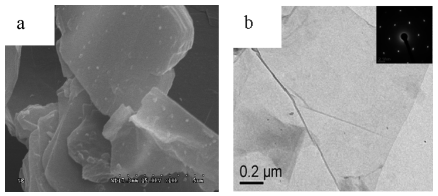

Figure 2. (a) SEM and (b) TEM images of GO.

that concurrently leads to GO exfoliation and dispersion to prepare PP/GO nanocomposite.

Preparation and Characterization of GO-Supported Ziegler−Natta Catalyst. Graphene oxide was prepared from natural graphite by the Hummers method.[1a] The as-prepared powdery GO contained 57.84 wt % of C and 1.82 wt % of H from the element analysis measurement. As high as 40.44 wt % of O could be calculated based on the content of C and H in GO, indicating that the degree of oxidation was very high.

The morphology of GO was studied with scanning electron microscopy (SEM) analysis (Figure 2a). Obviously, layered structure of GO was retained, which is in agreement with the literature reports.[1e,12] To further characterize the structure of GO, we conducted TEM analysis of cast film samples at the concentration of 1.0 mg/mL in THF. The TEM image of GO (Figure 2b) indicates that GO was fully exfoliated into nanosheets with micrometer-long wrinkles by ultrasonic treatment, exhibiting clearly a flake-like shape of graphene oxide, which is also consistent with the previous reports in the literature.[1e,13] The inset is the measured electron diffraction pattern of the GO nanosheet, showing diffraction dots. This confirms the highly crystalline signature of few-layered graphene oxide sheets.

In the late 1980s, Munoz-Escalona et al.[14] and Nowlin et al.[15] separately used Grignard reagent (BuMgCl and EtMgCl in THF) to react with hydroxyl groups of thermally treated SiO_2 and obtained RMgCl/SiO_2 support, and then $TiCl_4$ was supported on RMgCl/SiO_2 to synthesize

(12) (a) Jeong, H. K.; Jin, M. H.; An, K. H.; Lee, Y. H. *J. Phys. Chem. C* **2009**, *113*, 13060–13064. (b) Chang, C. C.; Liu, S. J.; Wu, J. J.; Yang, C. H. *J. Phys. Chem. C* **2007**, *111*, 16423–16427.
(13) (a) Yang, Y.; Wang, J.; Zhang, J.; Liu, J.; Yang, X.; Zhao, H. *Langmuir* **2009**, *25*(19), 11808–11814. (b) Li, Y.; Tang, L.; Li, J. *Electrochem. Commun.* **2009**, *11*, 846–849. (c) Du, X.; Yu, Z. Z.; Dasari, A.; Ma, J.; Mo, M.; Meng, Y.; Mai, Y. W. *Chem. Mater.* **2008**, *20*, 2066–2068. (d) Xu, Y.; Bai, H.; Lu, G.; Li, C.; Shi, G. *J. Am. Chem. Soc.* **2008**, *130*, 5856–5857.
(14) Munoz-Escalona, A.; Fuentes, A.; Liscano, J.; Albornoz, A. In *Studies in Surface Science and Catlaysis 56* Keii,T., Soga, K., Eds.; Kodansh: Tokyo, 1990; pp 377−393.
(15) Nowlin, E.; Kissin, Y. V.; Wagner, K. P. *J. Polym. Sci., Part A: Polym. Chem.* **1988**, *26*, 755–764.

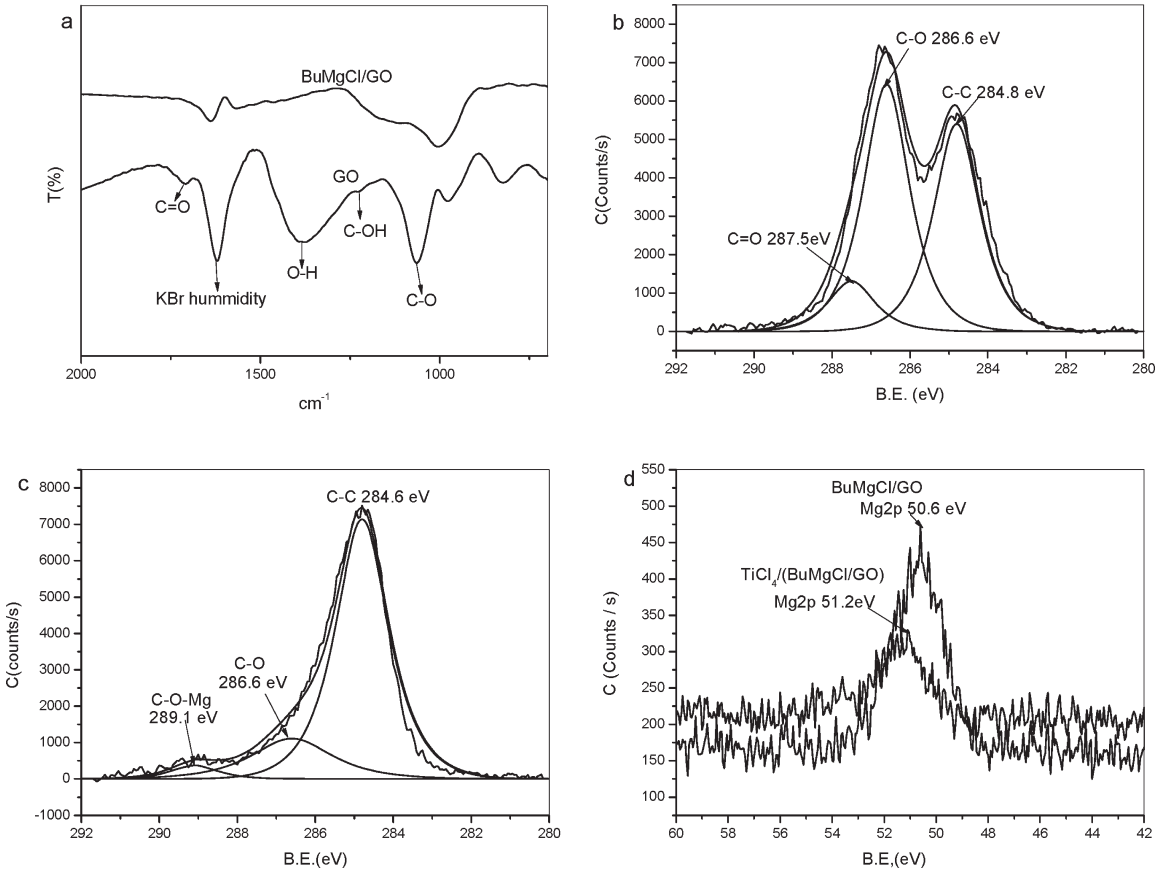

Figure 3. (a) FTIR spectra of GO and BuMgCl treated GO (BuMgCl/GO). (b) C 1s XPS spectra of GO, (c) C 1s XPS spectra of BuMgCl/GO, and (d) Mg 2p XPS spectra of BuMgCl/GO and $TiCl_4$/(BuMgCl/GO).

the $TiCl_4$/(RMgCl/SiO_2) catalyst for propylene polymerization. Recently, it was reported that graphene oxide in THF could be exfoliated mostly into individual nanosheets with lateral dimensions between a few hundred nanometers and a few micrometers.[16] As such, it can be reasonably expected that GO bearing hydroxyl, epoxide, and carboxyl polar groups without surface modification can be efficiently treated with the Grignard reagent (BuMgCl) in THF to synthesize the $TiCl_4$/(BuMgCl/GO) catalyst for propylene polymerization.

The treatment of GO with Grignard reagent BuMgCl in THF can lead to the derivation of the oxygen-containing groups via the formation of −O−Mg−Cl bond.[14,15,17] The chemical changes occurring upon the treatment of GO with BuMgCl were detected by FTIR spectroscopy (Figure 3a). After treatment with BuMgCl in THF, both the C═O stretching vibration at 1703 cm^{-1} and the O−H deformations at 1386 cm^{-1} in GO[16,18] disappeared and a strong absorption at 1004 cm^{-1} attributed to the C−O stretching appeared, indicating the chemical reaction between GO and BuMgCl.

GO, BuMgCl/GO, and $TiCl_4$/(BuMgCl/GO) were characterized by XPS, with the spectra shown in Figure 3b−d. The C 1s XPS spectrum of GO clearly indicates a considerable degree of oxidation with three components corresponding to carbon atoms in different functional groups: the nonoxygenated ring C (284.8 eV), the C in C−O bonds (286.6 eV), and the carboxylate carbon (C═O, 287.5 eV,).[13d,16] The two maxima in the C 1s band in Figure 3b are separated by −1.8 eV, and the complex C 1s bands of GO (Figure 3b) transforms into a relatively narrow and asymmetric band of BuMgCl/GO (Figure 3c). The C 1s bands located at 286.6 eV of GO became obscure, and the band at 289.1 eV is obviously seen in Figure 3c after GO was treated with BuMgCl. This can be attributed to the fact that the oxygen-containing functional groups were reacted with BuMgCl. As a result, the individual components of a given XPS band arising from different environments shift to different extents so that the −MgCl band is introduced into the band, indicating the reaction of GO with BuMgCl was highly effective. Furthermore, it can be seen from Figure 3d that the Mg 2p band of BuMgCl/GO located at 50.6 eV slightly shifts to higher binding energy (51.2 eV) after treatment with $TiCl_4$, which can be reasoned by chlorine in $TiCl_4$ coordinating with magnesium of the BuMgCl/GO (see Figure 1).[14,15] This indicates that $TiCl_4$ has been successfully supported on the BuMgCl/GO.

(16) Paredes, J. I.; Villar-Rodil, S.; Martínez-Alonso, A.; Tascón, J. M. D. *Langmuir* **2008**, *24*, 10560–10564.
(17) Xing, Q.; Fei, W.; Xu., R.; Fei, J. *Organic Chemistry*, 3rd ed; Advanced Education Press: Beijing, China, 2005; Vol. *12*. p 296.
(18) (a) Hontoria-Lucas, C.; Lopez-Peinado, A. J.; Lopez-Gonzalez, J. D.; Rojas-Cervantes, M. L.; Martin-Aranda, R. M. *Carbon* **1995**, *33*, 1585–1592. (b) Bourlinos, A. B.; Gournis, D.; Petridis, D.; Szabo, T.; Szeri, A.; Dekany, I. *Langmuir* **2003**, *19*, 6050–6055. (c) Szabo, T.; Berkesi, O.; Dekany, I. *Carbon* **2005**, *43*, 3186–3189. (d) Titelman, G. I.; Gelman, V.; Bron, S.; Khalfin, R. L.; Cohen, Y.; Bianco-Peled, H. *Carbon* **2005**, *43*, 641–649.

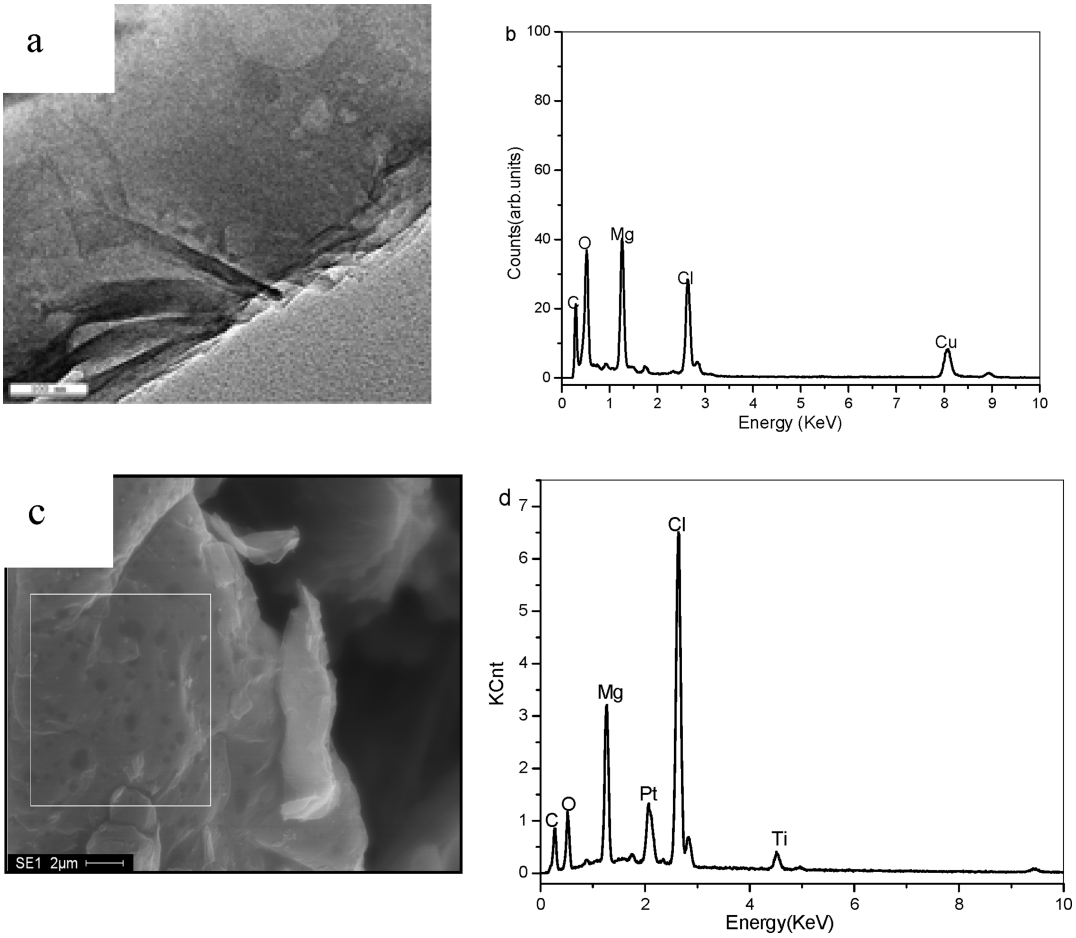

Figure 4. (a) TEM image of BuMgCl/GO, (b) the corresponding EDX spectrum of BuMgCl/GO (part a), (c) SEM image of $TiCl_4$/(BuMgCl/GO) catalyst, and (d) EDS spectrum of $TiCl_4$/(BuMgCl/GO) at an area indicated with a white line in part c.

TEM image of BuMgCl/GO is shown in Figure 4a. Its energy-dispersive X-ray (EDX) spectroscopy is presented in Figure 4b. GO after treatment with BuMgCl is still flaky, and strong peaks of Mg and Cl are presented in addition to C and O, indicating the reaction of GO with BuMgCl was successful, which is consistent with the results of the FITR and XPS analyses.

Figure 4c shows the SEM image of the $TiCl_4$/(BuMgCl/GO) catalyst, which exhibits clearly chip stacking replicating the morphology of the original GO. The energy-dispersive X-ray (EDX) spectroscopy of the $TiCl_4$/(BuMgCl/GO) catalyst for a selected area indicated in Figure 4c with a white square indicates that the transition metal Ti was successfully supported on the GO carrier in addition to C, O, Mg, and Cl (Figure 4d).

Because the oxygen-containing groups of GO (including carboxyl, hydroxyl and epoxide) are apt to decompose under high temperature,[3a,7b,c,16] the main mass loss (~60 wt %) of GO took place at around 260 °C (Figure 5A-a). However, BuMgCl/GO exhibits a greatly improved thermal stability (Figure 5A-b). The reason for this could be that the thermally stable −C−O−Mg−Cl group substitutes the carboxyl, hydroxyl, and epoxide groups of GO during the treatment of GO with BuMgCl. The final $TiCl_4$/(BuMgCl/GO) catalyst presents higher thermal stability compared with the original GO and the BuMgCl/GO precursor (Figure 5A).

To measure the intragallery spacing of GO before and after the treatment with $TiCl_4$/BuMgCl, wide angle XRD analyses were conducted (Figure 5B). GO has a prominent, characteristic diffraction peak at 13.6° of 2θ (Figure 5B-a), corresponding to the intragallery spacing of 0.65 nm. Both BuMgCl/GO and $TiCl_4$/(BuMgCl/GO) present several peaks in the range of 2θ from 1.5° to 60°. Compared to GO, the d_{001} diffraction peak of BuMgCl/GO (Figure 5B-b) shifts to lower angle and reaches $2\theta = 7.14°$, corresponding to the intragallery distance of 1.20 nm, which is 0.55 nm larger than that of GO before BuMgCl treatment, indicating the intercalation of BuMgCl into intragallery of GO and the elimination of some unsteady functional groups causing the interlayer distances to contract. The d_{001} diffraction peak of the $TiCl_4$/(BuMgCl/GO) catalyst (Figure 5B-c) is similar to that of BuMgCl/GO (Figure 5B-b), implying that the intragallery did not change after $TiCl_4$ was supported on the BuMgCl/GO.

In Situ Propylene Polymerization with GO-Supported Ziegler−Natta Catalyst. Propylene polymerization was performed with the $TiCl_4$/(BuMgCl/GO) catalyst, and the results are summarized in Table 1. For $TiCl_4$/(BuMgCl/GO), catalyst activities were in the range of 0.35×10^7-5.0×10^7 g PP/mol Ti per hour, depending on the [TEA]/[Ti] ratio used during the polymerization. Generally, higher [TEA]/[Ti] resulted in higher activity. The thermal properties

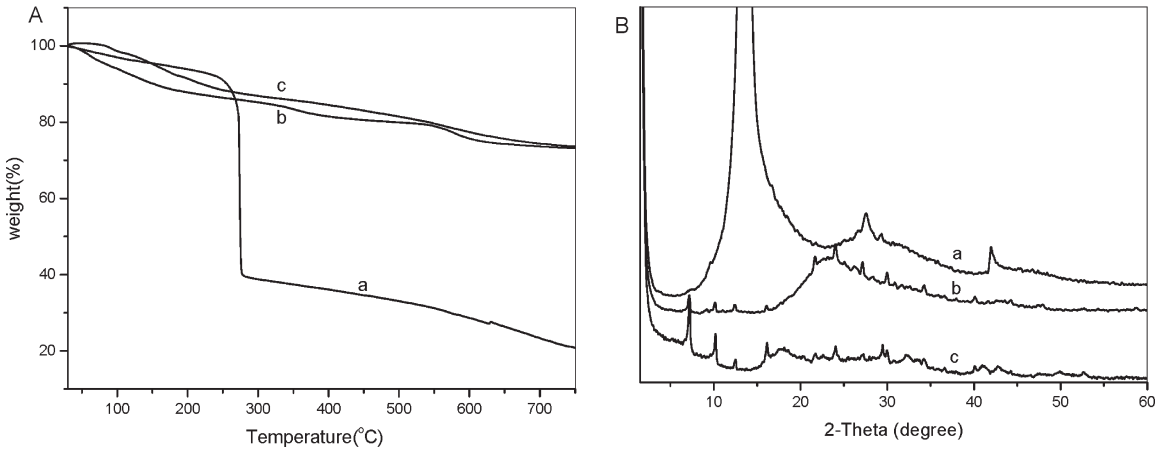

Figure 5. (A) TGA plots of (a)GO, (b) BuMgCl/GO, and (c) $TiCl_4$/(BuMgCl/GO); (B) XRD patterns of (a) GO, (b) BuMgCl/GO, and (c) $TiCl_4$/(BuMgCl/GO).

of the obtained PP/GO nanocomposites were studied by DSC. A consistent polymer melting temperature near 160 °C is reassuring. As can be seen in Table 1, the PP/GO nanocomposites with GO loading range of 0.42−4.90 wt % (calculated based on the added GO amount) were obtained in high yields.

To estimate the average molecular weight of the PP matrix, a nonthorough solvent extraction using xylene at 140 °C was conducted on the obtained hybrids. The retrieved GO-free polymer samples were subjected to viscosity measurement to determine their molecular weights (M_η), the results of which are included in Table 1. In the four PP/GO nanocomposites, the viscosity-average molecular weights of the PP matrixes are in the range of 7.3×10^5 g/mol to 8.1×10^5 g/mol, which are fairly high. It seems that by using the $TiCl_4$/(BuMgCl/GO) catalyst, the presence of GO did not affect the propagation of PP chains.

Morphological Characterization and Thermal and Electrical properties of PP/GO Nanocomposites. The dispersion of the GO nanosheets was evaluated by observing the fracture surface of the hybrids with SEM. It is seen that the GO sheets were dispersed well through the polymer matrix (Figure 6c−e). With GO present, the smooth surface of neat polypropylene (Figure 6b) becomes rough. Moreover, with the increase of GO content in hybrid, GO sheet layers gradually become visible in the fracture surface. At a GO content of 1.52 wt %, it seems that the hybrid is almost entirely filled with GO nanosheets (Figure 6e), which could be attributed to the extremely large surface of the GO sheets.

Transmission electron microscopy can also be used to evaluate the exfoliation and dispersion quality of GO in polymers.[3a,e,f,8b,9,13c] Figure 3f is a high-resolution transmission electron microscopy (HR-TEM) image of the sample PP1 with 0.96 wt % of GO, showing that each flake is composed of few-layered sheets in PP matrix. The electron diffraction pattern of the sample presents spot patterns matching those of individual GO nanosheets. The GO flakes in our study are composed of such stacked individual sheets, seen in Figure 2b. Furthermore, it can be clearly seen that graphene sheets of GO (indicated with white arrows) are corrugated from the TEM images of

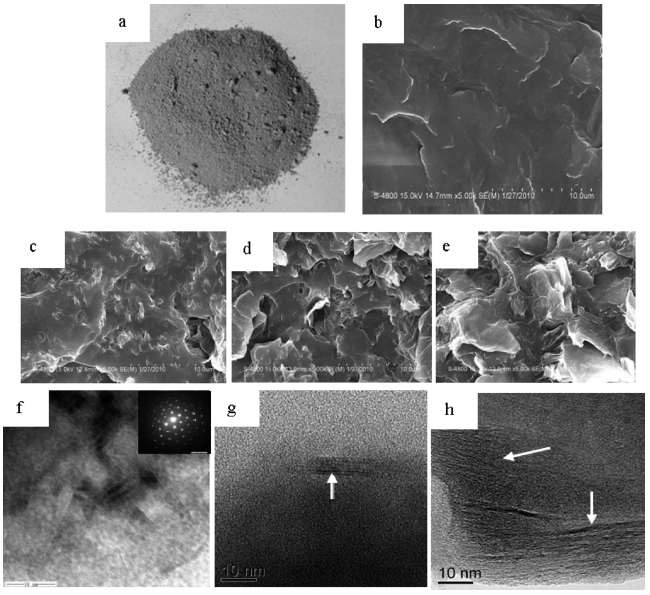

Figure 6. (a) PP/GO nanocomposites powder as obtained after coagulation in ethanol (containing 0.1 M HCl). (b) SEM images obtained from fracture surface of neat PP without GO. (c−e) SEM images obtained from fracture surface of composite samples of 0.42, 1.52, and 4.90 wt %, respectively, GO loadings. (f) TEM image of sample PP1 with 0.96 wt % of GO (the inset showing the measured electron diffraction pattern). (g) TEM image of sample PP3 with 1.52 wt % of GO. (h) TEM image of sample PP4 with 4.90 wt % of GO.

sample PP3 with 1.52 wt % GO (Figure 6g) and PP4 with 4.90 wt % GO (Figure 6h), indicating that GO nanosheets are well exfoliated in PP matrix. In all, we deduce that the graphene oxide nanosheets are well exfoliated and homogenously dispersed in the PP matrix from the SEM and TEM images.

The conducting feature of graphene motivated the conductivity measurement of the PP nanocomposites although GO was reported to have a much lower electrical conductivity than graphene. The polymerized samples were compressed to be films with thickness around 0.3−0.5 mm at 190 °C for electrical conductivity measurement. Under the processing temperature of 190 °C, GO cannot be thermally reduced to graphene.[11] The electrical conductivities for the PP/GO nanocomposites are

listed in Table 1. At a loading of about 1.52 wt %, the electrical conductivity of PP/GO nanocomposite film already satisfies the antistatic criterion (10^{-6} S m^{-1}).[19] Generally speaking, a rapid increase in the direct current electrical conductivity of polymer composites implies the formation of a conducting network throughout the insulating polymer matrix.[3a,b,20] A 4.90 wt % of GO loading results in an electrical conductivity as high as 0.3 S m^{-1}. It is interesting to note that the GO used in this study was not reduced intentionally by a reducing agent; however, the resulting nanocomposites were still highly electrically conductive, which may be, tentatively, attributed to the network between PP matrix and GO through chemical bonding that contribute to generating electrically conductive pathway in the nanocomposites.[20a]

Conclusions

In summary, PP/GO nanocomposites are prepared via in situ intercalative polymerization using Ziegler−Natta catalyst, which was made possible by preparing a supported catalyst system primarily structured by nanoscale, predominantly single GO sheet. This approach overcomes the incompatibility barricade between the polar graphene oxide and nonpolar PP matrix that prevents the exfoliation and dispersion of GO nanosheets in PP matrix. The GO nanosheets are found to be well exfoliated and homogenously dispersed in the PP matrix from the TEM and SEM images. High electrical conductivity is discovered with thus prepared PP/GO nanocomposites, for example, at a GO loading of 4.9 wt %, σ_c has been measured at 0.3 S m^{-1}. More detailed studies of the structure and properties of the in situ polymerized PP/GO nanocomposites of varied compositions are being undertaken in our laboratory, the results of which will be reported elsewhere. Moreover, we are also trying to apply the same chemistry to prepare other polyolefin/GO nanocomposites.

Acknowledgment. Financial support by the National Science Foundation of China (Grants 20734002 and 20874104), Ministry of Science and Technology of China (863 project, Series 2008AA030901 and 2009AA033601), and Chinese Academy of Sciences (Directional key project on high-performance polypropylene alloy resin development) are gratefully acknowledged.

Supporting Information Available: DSC traces of PP/GO nanocomposites of various GO loadings. This information is available free of charge via the Internet at http://pubs.acs.org/.

(19) Chung, D. D. L. *J. Mater. Sci.* **2004**, *39*, 2645–2661.
(20) (a) Lee, S. H.; Cho, E.; Jeon, S. H.; Youn, J. R. *Carbon* **2007**, *45*, 2810–2822. (b) Micušik, M.; Omastová, M.; Krupa, I.; Prokeš, J.; Pissis, P.; Logakis, E.; Pandis, C.; Potschke, P.; Pionteck, J. *J. Appl. Polym. Sci.* **2009**, *113*, 2536–2551. (c) King, J. A.; Johnson, B. A.; Via, M. D.; Ciarkowski, C. J. *J. Appl. Polym. Sci.* **2009**, *112*, 425–433.